

Kondo screening cloud in a superconductor with mixed s-wave and p-wave pairing states

Zhen-Zhen Huang(黄真真), Xiong-Tao Peng(彭雄涛), Wan-Sheng Wang(王万胜), and Jin-Hua Sun(孙金华)
Citation: Chin. Phys. B, 2022, 31 (**10**): 107101. DOI: 10.1088/1674-1056/ac7213
Journal homepage: http://cpb.iphy.ac.cn; http://iopscience.iop.org/cpb

What follows is a list of articles you may be interested in

Uniaxial stress effect on quasi-one-dimensional Kondo lattice $CeCo_2Ga_8$

Kangqiao Cheng(程康桥), Binjie Zhou(周斌杰), Cuixiang Wang(王翠香), Shuo Zou(邹烁), Yupeng Pan(潘宇鹏), Xiaobo He(何晓波), Jian Zhang(张健), Fangjun Lu(卢方君), Le Wang(王乐), Youguo Shi(石友国), and Yongkang Luo(罗永康)
Chin. Phys. B, 2022, 31 (**6**): 067104. DOI: 10.1088/1674-1056/ac6339

Resistivity minimum emerges in Anderson impurity model modified with Sachdev-Ye-Kitaev interaction

Lan Zhang(张欄), Yin Zhong(钟寅), and Hong-Gang Luo(罗洪刚)
Chin. Phys. B, 2021, 30 (**4**): 047106. DOI: 10.1088/1674-1056/abefcb

Intercalation of van der Waals layered materials: A route towards engineering of electron correlation

Jingjing Niu(牛晶晶), Wenjie Zhang(章文杰), Zhilin Li(李治林), Sixian Yang(杨嗣贤), Dayu Yan(闫大禹), Shulin Chen(陈树林), Zhepeng Zhang(张哲朋), Yanfeng Zhang(张艳锋), Xinguo Ren(任新国), Peng Gao(高鹏), Youguo Shi(石友国), Dapeng Yu(俞大鹏), Xiaosong Wu(吴孝松)
Chin. Phys. B, 2020, 29 (**9**): 097104. DOI: 10.1088/1674-1056/abab85

Benchmarking the simplest slave-particle theory with Hubbard dimer

Wei-Wei Yang(杨薇薇), Hong-Gang Luo(罗洪刚), Yin Zhong(钟寅)
Chin. Phys. B, 2019, 28 (**10**): 107103. DOI: 10.1088/1674-1056/ab3dfe

Voltage-controlled Kosterlitz-Thouless transitions and various kinds of Kondo behaviors in a triple dot device

Yong-Chen Xiong(熊永臣), Jun Zhang(张俊), Wang-Huai Zhou(周望怀), Amel Laref
Chin. Phys. B, 2017, 26 (**9**): 097102. DOI: 10.1088/1674-1056/26/9/097102

Kondo screening cloud in a superconductor with mixed s-wave and p-wave pairing states

Zhen-Zhen Huang(黄真真), Xiong-Tao Peng(彭雄涛), Wan-Sheng Wang(王万胜), and Jin-Hua Sun(孙金华)†

School of Physical Science and Technology, Ningbo University, Ningbo 315211, *China*

(Received 3 April 2022; revised manuscript received 17 May 2022; accepted manuscript online 23 May 2022)

We study the Kondo screening of a spin-1/2 magnetic impurity coupled to a superconductor, which is fabricated by combination of an s-wave superconductor, a ferromagnet and a semiconductor with Rashba spin–orbit coupling (RSOC). The proximity induced superconducting states include the s-wave and p-wave pairing components with the aids of RSOC, and the ferromagnet induces a Zeeman field which removes the spin degeneracy of the quasiparticles in the triplet states. Thus, the Kondo screening of magnetic impurity involves the orbital degrees of freedom, and is also affected by the Zeeman field. Using the variational method, we calculate the binding energy and the spin–spin correlation between the magnetic impurity and the electrons in the coexisting s-wave and p-wave pairing states. We find that Kondo singlet forms more easily with stronger RSOC, but Zeeman field in general decreases the binding energy. The spin–spin correlation decays fast in the vicinity of the magnetic impurity. Due to the RSOC, the spatial spin–spin correlation becomes highly anisotropic, and the Zeeman field can induce extra asymmetry to the off-diagonal components of the spin–spin correlation. Our study can offer some insights into the studies of extrinsic topological superconductors fabricated from the hybrid structures containing chains of magnetic impurities.

Keywords: Kondo effect, Rashba spin–orbit couplings, p-wave superconductors, Anderson model

PACS: 71.20.Be, 75.20.Hr, 03.65.Vf, 71.27.+a **DOI:** 10.1088/1674-1056/ac7213

1. Introduction

The Kondo effect arises when local magnetic impurity spins couple antiferromagnetically with conduction electron spins. As a prototypical strong correlation problem, Kondo effect in normal metals has been widely studied and well understood.[1,2] If the temperature is above the so-called Kondo temperature $T_{\rm K}$, the magnetic impurities can be treated perturbatively. However, at temperatures well below $T_{\rm K}$, perturbation theory fails, and it has been confirmed, using the numerical renormalization group study, that the magnetic impurity spins are entirely screened by the conduction electron spins.[3]

When the magnetic impurity couples to an s-wave superconductor, the low-energy transport is dominated by the spin-induced Yu–Shiba–Rusinov (YSR) state,[4–6] which is determined by the competition between the Kondo effect and the superconductivity. The ground state will be a Kondo singlet if $T_{\rm K} > \Delta$, otherwise the ground state will be a magnetic doublet if $T_{\rm K} < \Delta$, where Δ is the superconducting gap. The interest in magnetic doping in superconductors persists because it can provide information to understanding the properties of superconducting states. The properties of YSR states is one of the major methods to characterize the pairing symmetry of the superconducting states, and has been widely studied in the high-temperature cuprate superconductors,[7–10] iron-based superconductors,[11–13] chiral p-wave superconductors,[14,15] topological superconductors,[16,17] nematic superconductors,[18] etc. More recently, the pairing symmetry dependent YSR states are studied in the superconducting phase of twisted bilayer graphene.[19]

Besides the YSR states, the formation of the Kondo screening cloud, which is characterized by the spin–spin correlation function between the magnetic impurity and the conduction electrons, is also a fascinating problem. In a D-dimensional normal metal, the spin–spin correlation function follows a power law decay $1/r^D$ if $r < \xi_{\rm K}$, but $1/r^{D+1}$ if $r > \xi_{\rm K}$, with $\xi_{\rm K}$ being the Kondo coherence length.[20–22] Numerical renormalization group study shows that in an s-wave superconductor, the Kondo screening cloud is formed in both the screened and unscreened phases, and decays with respect to $1/r$ in the vicinity of the magnetic impurity, and the decay rate in larger distances depends on the magnitude of the superconducting gap.[23] Note that the signatures of the Kondo screening cloud extending over a length of micrometers has been confirmed recently via Fabry–Pérot oscillations in conductance.[24]

In unconventional superconductors, the magnetic impurity behavior is more complicated. Numerical renormalization group study shows that despite sharing the p + ip pairing symmetry, intrinsic and extrinsic topological superconductors host different physical processes that produce distinct Kondo signatures.[25] The magnetic doping in the intrinsic p-wave pairing states corresponds to a strong spin doublet ground state with partially screened magnetic impurity spin. In the extrinsic p-wave pairing states, the Kondo screening involves both

†Corresponding author. E-mail: sunjinhua@nbu.edu.cn

© 2022 Chinese Physical Society and IOP Publishing Ltd

the electron and orbital degrees of freedom to produce rich and prominent Kondo phenomena. In the presence of Rashba spin–orbit coupling (RSOC), the YSR state exhibits Zeeman-dependent splitting behaviors.[26]

The purpose of this paper is to investigate the properties of the binding energy and the spatial Kondo screening cloud in a superconductor with coexisting s-wave and p-wave pairing states. The variational method we apply has been used to study the ground state of the Kondo problem in normal metals,[27,28] antiferromagnet,[29] 2D helical metals,[30] various 3D topological semimetals.[31–35] It has also been applied to study the magnetic impurity effects in the s-wave and d-wave superconductors.[36–39] Due to the combined effects of the RSOC and the Zeeman field, the Kondo screening cloud is expected to show very interesting features, such as the spatial anisotropy and the emergence of the off-diagonal components of the spin–spin correlation function.

The paper is organized as follows. We introduce the Anderson model Hamiltonian in Section 2. In Section 3, we apply the variational method to study the binding energy. In Section 4, we investigate the spin–spin correlation between the magnetic impurity and the conduction electrons in the superconductor with coexisting s-wave and p-wave pairing states. Finally, the discussions and conclusions are given in Section 5.

2. Anderson model Hamiltonian

The mixed s-wave and p-wave pairing states can be generated in a heterostructure fabricated by a combination of an s-wave superconductor and the two-dimensional electron gas (2DEG) with RSOC.[40–42] The Zeeman field induced by the ferromagnetic insulator can significantly alter the superconducting states, and even lead to a topological phase transition.[43,44]

We use the well-known Anderson impurity model to study the Kondo screening of a spin-1/2 magnetic impurity coupled to the mixed s-wave and p-wave pairing states. The Anderson model Hamiltonian reads

$$H = H_0 + H_{\rm d} + H_{\rm V}. \tag{1}$$

$H_0 = H_{\rm RSOC} + H_{\rm s} + H_z$ describes the host material with coexisting spin singlet and triplet pairing states, $H_{\rm d}$ is the magnetic impurity Hamiltonian, and $H_{\rm V}$ is the hybridization between the magnetic impurity and the conduction electrons of the superconducting host. $H_{\rm RSOC}$ describes the 2DEG with the RSOC,

$$H_{\rm RSOC} = \sum_{\boldsymbol{k}\sigma} \varepsilon_{\boldsymbol{k}} c^{\dagger}_{\boldsymbol{k}\sigma} c_{\boldsymbol{k}\sigma} + \sum_{\boldsymbol{k}} \lambda \boldsymbol{k} (\mathrm{e}^{-\mathrm{i}\theta_k} c^{\dagger}_{k\downarrow} c_{k\uparrow} + \mathrm{H.c.}), \tag{2}$$

where $\varepsilon_{\boldsymbol{k}} = \frac{\boldsymbol{k}^2}{2m} - \mu$ is the kinetic energy term and μ is the chemical potential; $c_{\boldsymbol{k}\sigma}$ ($c^{\dagger}_{\boldsymbol{k}\sigma}$) are the annihilation (creation) operators for electrons with spin $\sigma = \uparrow, \downarrow$ and the momentum $\boldsymbol{k} = (k_x, k_y)$; λ describes the strength of the RSOC; and $\theta_k = \arctan(k_x/k_y)$ is the polar component of $\boldsymbol{k}$ with $k = |\boldsymbol{k}|$. $H_{\rm s}$ denotes the Hamiltonian of proximity-induced superconducting pairing interaction

$$H_{\rm s} = -\sum_{\boldsymbol{k}} (\Delta c^{\dagger}_{\boldsymbol{k}\uparrow} c^{\dagger}_{-\boldsymbol{k}\downarrow} + \mathrm{H.c.}), \tag{3}$$

with Δ being the proximity-induced gap. The out-of-plane Zeeman splitting is given by

$$H_z = \sum_{\boldsymbol{k}\sigma} \sigma_z v_z c^{\dagger}_{\boldsymbol{k}\sigma} c_{\boldsymbol{k}\sigma}. \tag{4}$$

σ_z is the z-component of the spin Pauli matrix. The p-wave pairings can be induced in the 2DEG with the aids of RSOC and s-wave pairing states.[40–42] In fact, the Zeeman field shall couple both to the spins of the bulk electrons and to the d-electrons, depending on the g factors which need not be equal for the two cases. It is well-known that the spin degeneracy of the impurity energy level shall be lifted by the Zeeman field, leading to a Kondo peak splitting. However, to eliminate the additional complexity caused by the Zeeman splitting of the impurity energy level and mainly concentrate on the interplay between the Kondo effect and the mixed s- and p-wave pairing states, we assume that the g factor for the magnetic impurity is zero. This case has been discussed before[26,45,46] and seems to be achievable in quantum dots.[47] The Hamiltonian of the magnetic impurity is

$$H_{\rm d} = \sum_{\sigma} \varepsilon_{\rm d} d^{\dagger}_{\sigma} d_{\sigma} + U n_{\uparrow} n_{\downarrow}, \tag{5}$$

where $\varepsilon_{\rm d}$ is impurity level and U is Coulomb repulsion, d_{σ} is the annihilation operator of magnetic impurity electrons, and $n_{\sigma} = d^{\dagger}_{\sigma} d_{\sigma}$. The hybridization between the magnetic impurity and the superconductor is

$$H_{\rm V} = \sum_{\boldsymbol{k}\sigma} (V c^{\dagger}_{\boldsymbol{k}\sigma} d_{\sigma} + \mathrm{H.c.}), \tag{6}$$

where V is the hybridization strength. For simplicity, we set the position of the impurity as the origin $\boldsymbol{r} = 0$, so that the hybridization V is in fact independent of spin and momentum.

To deal with the RSOC term and the superconducting pairings, we switch to a continuum representation

$$c_{\boldsymbol{k}\sigma} = \sqrt{\frac{2\pi}{k}} \sum_{m=-\infty}^{\infty} \mathrm{e}^{\mathrm{i}m\theta_k} c^{m}_{k\sigma}, \tag{7}$$

where m is the orbital magnetic quantum number. The operator $c^{m\dagger}_{k\sigma}$ ($c^{m}_{k\sigma}$) obeys the canonical anticommutation relation $\{c^{m}_{k\sigma}, c^{m'\dagger}_{k'\sigma'}\} = \delta(k-k')\delta_{mm'}\delta_{\sigma\sigma'}$. H_0 can be diagonalized by performing the canonical transformation

$$c_{hkm+1/2} = \frac{1}{\sqrt{2}} (\beta_{hk} c^{m}_{k\uparrow} + h\beta_{-hk} c^{m+1}_{k\downarrow}), \tag{8}$$

with $\beta_{hk} = (1 + hv_z/\sqrt{\lambda^2 k^2 + v_z^2})^{1/2}$, and $h = \pm 1$ is the chirality quantum number.[46,48]

Finally, the superconductor with mixed s-wave and p-wave states reads

$$H_0 = \sum_{hm} \int \mathrm{d}k \varepsilon_{hk} c^{\dagger}_{hkm+\frac{1}{2}} c_{hkm+\frac{1}{2}}$$

$$-\frac{\Delta}{2}\sum_{hh'm}\int \mathrm{d}k(\beta_{-hk}\beta_{h'k}hc^{\dagger}_{hkm-1/2}c^{\dagger}_{h'-k-m+1/2} +\mathrm{H.c.}), \quad (9)$$

with $\varepsilon_{hk}=\varepsilon_k+h\sqrt{\lambda^2k^2+v_z^2}$ and $\sum_{\boldsymbol{k}}=1/4\pi^2\int k\mathrm{d}k\mathrm{d}\theta_k$ in the derivation. In the presence of RSOC, both the spin and orbital angular momentum are not good quantum numbers, while the total angular momentum $j=m+\sigma$ is a conserved quantity.[46,48–50] Here, the pairing is s-wave pairing when $h=-h'$, and p-wave pairing when $h=h'$.[51–54] Then the hybridization term can be rewritten as

$$H_{\mathrm{V}}=\sum_{hj}\int \mathrm{d}k\tilde{V}(h^{-j+1/2}\beta_{\mathrm{sign}(j)hk}c^{\dagger}_{hkj}d_{\downarrow}+\mathrm{H.c.}), \quad (10)$$

where $\tilde{V}=\sqrt{\frac{k}{4\pi}}V$, and $\mathrm{sign}(j)=\pm1$ for $j=\pm1/2$. We assume the short range scattering such that only the $m=0$ electrons are directly coupled to the magnetic impurity.

Introducing the Nambu representation $\psi(k)=(c_{1k\frac{1}{2}},c^{\dagger}_{1-k-\frac{1}{2}},c^{\dagger}_{-1-k-\frac{1}{2}},c_{-1k\frac{1}{2}})^{\mathrm{T}}$, and considering only the $j=\pm1/2$ terms, the Bogoliubov–de Gennes (BdG) Hamiltonian H_0 can be rewritten as $H_0=\int \mathrm{d}k\psi^{\dagger}(k)h_0(k)\psi(k)$, where

$$h_0(k)=\begin{pmatrix}\varepsilon_{1k} & 0 & -\Delta & 0\\ 0 & -\varepsilon_{1-k} & 0 & \Delta\\ -\Delta & 0 & -\varepsilon_{-1-k} & 0\\ 0 & \Delta & 0 & \varepsilon_{-1k}\end{pmatrix}. \quad (11)$$

By diagonalizing $h_0(k)$, one can easily obtain four eigenvalues as $\pm\sqrt{\lambda^2k^2+v_z^2}\pm\sqrt{\Delta^2+\varepsilon_k^2}$. We label the excitation energies in an increasing order as $E_{k2},E_{k3},E_{k4},E_{k1}$, such that H_0 in its diagonal basis reads

$$H_0=\int \mathrm{d}k(E_{k2}+E_{k3})+\int \mathrm{d}k(E_{k1}\gamma^{\dagger}_{\alpha k0}\gamma_{\alpha k0} -E_{k2}\gamma^{\dagger}_{\alpha k1}\gamma_{\alpha k1}-E_{k3}\gamma^{\dagger}_{\beta k1}\gamma_{\beta k1}+E_{k4}\gamma^{\dagger}_{\beta k0}\gamma_{\beta k0}). \quad (12)$$

The corresponding eigenstate operators are given by

$$\gamma(k)=\mathcal{U}\psi(k), \quad (13)$$

where $\gamma(k)\equiv\{\gamma_{\alpha k0},\gamma^{\dagger}_{\alpha k1},\gamma^{\dagger}_{\beta k1},\gamma_{\beta k0}\}^{\mathrm{T}}$. $\mathcal{U}$ is a unitary matrix formed from the eigenvectors, and the matrix elements are given in Appendix A.

Then, the hybridization part is given by

$$H_{\mathrm{V}}=\int \mathrm{d}k\tilde{V}\Big[\Big(A_1\gamma^{\dagger}_{\alpha k0}+A_2\gamma_{\alpha k1}+A_3\gamma_{\beta k1}+A_4\gamma^{\dagger}_{\beta k0}\Big)d_{\frac{1}{2}} +\Big(A_5\gamma_{\alpha k0}+A_6\gamma^{\dagger}_{\alpha k1}+A_7\gamma^{\dagger}_{\beta k1}+A_8\gamma_{\beta k0}\Big)d_{-\frac{1}{2}}+\mathrm{H.c.}\Big], \quad (14)$$

with

$$\begin{aligned}&A_1=\beta_{1k}\Phi_{11}+\beta_{-1k}\Phi_{41}, \quad A_2=\beta_{1k}\Phi_{12}+\beta_{-1k}\Phi_{42},\\ &A_3=\beta_{1k}\Phi_{13}+\beta_{-1k}\Phi_{43}, \quad A_4=\beta_{1k}\Phi_{14}+\beta_{-1k}\Phi_{44},\\ &A_5=\beta_{-1k}\Phi_{21}-\beta_{1k}\Phi_{31}, \quad A_6=\beta_{-1k}\Phi_{22}-\beta_{1k}\Phi_{32},\\ &A_7=\beta_{-1k}\Phi_{23}-\beta_{1k}\Phi_{33}, \quad A_8=\beta_{-1k}\Phi_{24}-\beta_{1k}\Phi_{34}. \quad (15)\end{aligned}$$

Note that spin is not a good quantum number, so we rewrite the impurity operators as $d_{\uparrow}\to d_{\frac{1}{2}}$, $d_{\downarrow}\to d_{-\frac{1}{2}}$.

3. The self-consistent calculation

To investigate the eigenstate property, we utilize a trial wavefunction approach. The Coulomb repulsion U is assumed to be large enough, and ε_{d} is below the Fermi energy, so that the impurity site is always singly occupied by a local moment. When a magnetic impurity is coupled to an s-wave superconductor, the ground state will be a Kondo singlet if $T_{\mathrm{K}}>\Delta$, otherwise the ground state will be a magnetic doublet if $T_{\mathrm{K}}<\Delta$, where Δ is the superconducting gap. The ground state is determined by the competition between T_{K} and Δ. However, quite distinctly, magnetic impurities in an intrinsic p-wave superconductor always form a magnetic doublet ground state. When the s- and p-wave pairings coexist, the ground state becomes very interesting, and a quantum phase transition from a magnetic doublet to a singlet ground state takes place as the RSOC increases.[26] In our calculations, we consider very large RSOC (λ) and hybridization strength (V) in comparison to the superconducting gap, and assume that the ground state is a Kondo singlet. The trial wavefunction is given by[36–39]

$$|S\rangle=\{a_0+\sum_k[a_{k\alpha}(d^{\dagger}_{1/2}\gamma^{\dagger}_{\alpha k1}-d^{\dagger}_{-1/2}\gamma^{\dagger}_{\alpha k0}) +a_{k\beta}(d^{\dagger}_{1/2}\gamma^{\dagger}_{\beta k1}-d^{\dagger}_{-1/2}\gamma^{\dagger}_{\beta k0})]\}|G\rangle, \quad (16)$$

where a_0, $a_{k\alpha}$, $a_{k\beta}$ are the variational parameters to be determined through self-consistent calculations. $|G\rangle$ is the ground state of the superconductor, and $\gamma_{\alpha ki}|G\rangle=\gamma_{\beta ki}|G\rangle=0$ ($i=0,1$). In fact, virtual excitations to the doubly occupied intermediate state can affect the spin exchange process in the Anderson model. Using the Schrieffer–Wolff transformation and to the lowest order of hybridization V, the Anderson model in the $n_{\mathrm{d}}=1$ subspace turns to be equivalent to the s–d exchange model with the effective couplings containing both the doubly occupied intermediate state and the singly occupied states. However, in strong repulsion limit, $U\to\infty$, the contribution of the doubly occupied intermediate state becomes negligible. Hence in the trial wavefuncion, we assume a singlet ground state with two terms: the first term describes the amplitude for the filled Fermi sea with an empty impurity site, and the second term with the summation over k describes the superposition of states with a singly occupied impurity level.

The energy E_{S} of the total Hamiltonian in the singlet state $|S\rangle$ is

$$\begin{aligned}E_{\mathrm{S}}\langle S|S\rangle&=\langle S|H|S\rangle\\ &=-\int \mathrm{d}k'(E_{k'1}+E_{k'4})\\ &\quad\times\left(a_0^2+\frac{1}{2\pi^2}\int k^2a_{k\alpha}^2\,\mathrm{d}k+\frac{1}{2\pi^2}\int k^2a_{k\beta}^2\,\mathrm{d}k\right)\\ &\quad+\frac{1}{2\pi^2}\int k^2\,\mathrm{d}k(E_{k1}a_{k\alpha}^2+E_{k4}a_{k\beta}^2)\end{aligned}$$

$$+\frac{\varepsilon_{\rm d}}{2\pi^2}\int k^2(a_{k\alpha}^2+a_{k\beta}^2)\,{\rm d}k$$
$$+\frac{1}{\pi}\int \tilde{V}a_0[(A_2-A_5)a_{k\alpha}$$
$$+(A_3-A_8)a_{k\beta}]k\,{\rm d}k. \quad (17)$$

According to the variational principle $\partial E_{\rm S}/\partial a_0 = \partial E_{\rm S}/\partial a_{k\alpha} = \partial E_{\rm S}/\partial a_{k\beta} = 0$, we obtain

$$E_{\rm S} = -\int {\rm d}k(E_{k1}+E_{k4}) + \frac{1}{2\pi}\int \tilde{V}[(A_2-A_5)a_{k\alpha}+(A_3-A_8)a_{k\beta}]\frac{1}{a_0}k\,{\rm d}k, \quad (18)$$

$$a_{k\alpha} = -\frac{\tilde{V}(A_2-A_5)\pi a_0}{k[E_{k1}-\int {\rm d}k'(E_{k'1}+E_{k'4})+\varepsilon_{\rm d}-E_{\rm S}]}, \quad (19)$$

$$a_{k\beta} = -\frac{\tilde{V}(A_3-A_8)\pi a_0}{k[E_{k4}-\int {\rm d}k'(E_{k'4}+E_{k'4})+\varepsilon_{\rm d}-E_{\rm S}]}. \quad (20)$$

Then the self-consistent equation is given by

$$E_{\rm S} = -\int {\rm d}k(E_{k1}+E_{k4}) + \frac{1}{2\pi}\int \tilde{V}[(A_2-A_5)a_{k\alpha}+(A_3-A_8)a_{k\beta}]k\,{\rm d}k. \quad (21)$$

We define the binding energy as $\Delta_{\rm b} = -\int {\rm d}k(E_{k1}+E_{k4})+\varepsilon_{\rm d}-E_{\rm S}$, then the self-consistent equation is given by

$$\varepsilon_{\rm d}-\Delta_{\rm b} = -\frac{\tilde{V}^2}{2}\int\left[\frac{(A_2-A_5)^2}{E_{k1}+\Delta_{\rm b}}+\frac{(A_3-A_8)^2}{E_{k4}+\Delta_{\rm b}}\right]{\rm d}k. \quad (22)$$

In all our calculations, $\Delta_0 = W/2500$ indicates a typical superconducting gap size, and W is the bandwidth far from the Fermi surface, such that the energy cutoff has minor impact on the low-energy physics. The chemical potential is fixed as $\mu = 0$, and the impurity energy level is slightly below the Fermi surface that $\varepsilon_{\rm d}-\mu = -\Delta_0/20$.

In Fig. 1 we show the self-consistent results of the binding energy of a superconductor with mixed s-wave and p-wave pairing states. The results are obtained by numerically solving Eq. (22). In Fig. 1(a) we show the self-consistent results of the binding energy $\Delta_{\rm b}$ with respect to hybridization V for $\Delta = \Delta_0$ for various combinations of parameters λ and v_z. We can see that with the increase of λ, the binding energy $\Delta_{\rm b}$ also increases, indicating that Kondo singlet is favored for large RSOC. The Kondo screening of a magnetic impurity in an otherwise clean 2DEG with RSOC has been studied in previous works using various methods, and it was shown that in general, the RSOC has weak influence on the Kondo temperature. The Kondo temperature displays a quasilinear dependence on the square of the RSOC with a slope that is positive for $\varepsilon_{\rm d}+U/2>0$, and negative for $\varepsilon_{\rm d}+U/2<0$.[46,48,49,55] There also exists another scenario for an isolated system with a constant band filling and a Fermi energy that varies with the RSOC, once the RSOC exceeds a critical value proportional to bottom of the bands in the absence of the RSOC, the system enters the helical metal regime and $T_{\rm K}$ rises rapidly.[46] However, the binding energy $\Delta_{\rm b}$ decreases for larger Zeeman field v_z. In general, for all the cases, $\Delta_{\rm b}$ increases monotonically with respect to V, indicating that the Kondo singlet states are more easily formed with larger hybridizations. This behavior is in general consistent with the results given in the s-wave superconductor. The formation of the ground state is determined by the competition between the Kondo temperature $T_{\rm K}$ and the superconducting gap Δ, and larger $T_{\rm K}$ corresponds to larger V. If the hybridization is strong enough, the ground state is always a Kondo singlet, while weak hybridization corresponds to the magnetic doublet ground state where the impurity remains partially screened. Figure 1(b) is the self-consistent results of the binding energy $\Delta_{\rm b}$ with respect to superconducting gap Δ for $V = 27.5\Delta_0$. As we can see, $\Delta_{\rm b}$ grows monotonically with λ, but decreases if v_z becomes larger. Furthermore, the binding energy $\Delta_{\rm b}$ reduces as the superconducting gap Δ increases, indicating that the larger the superconducting gap is, the more difficult it is for the impurity electrons to break the superconducting pair and form a Kondo singlet.

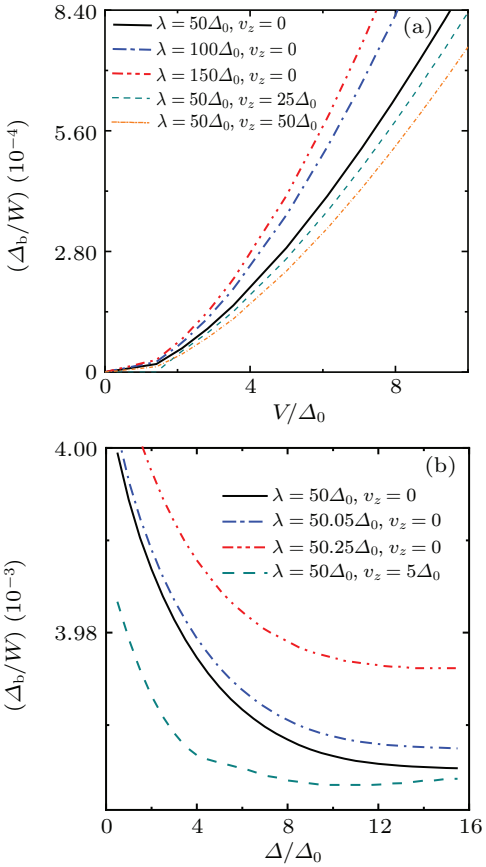


Fig. 1. Self-consistent results of the binding energy $\Delta_{\rm b}$ (a) with respect to hybridization V for $\Delta = \Delta_0$ and (b) with respect to superconducting gap Δ for $V = 27.5\Delta_0$. The results are given for various combinations of parameters λ, v_z, Δ. In all the calculations, $\Delta_0 = W/2500$ indicates a typical superconducting gap size, and the bandwidth and chemical potential are fixed at $W = 2500\Delta_0 \gg \Delta_0$ and $\mu = 0$.

4. The spin–spin correlation

In this section, we study the spatial spin–spin correlation between the magnetic impurity and the conduction electrons in the mixed s-wave and p-wave superconducting states. The spin operators of the magnetic impurity and conduction electrons in the superconductor are defined as $\boldsymbol{S}_{\rm d}=\frac{1}{2}d^{\dagger}\boldsymbol{\sigma}d$ and $\boldsymbol{S}_{\rm c}=\frac{1}{2}c^{\dagger}(\boldsymbol{r})\boldsymbol{\sigma}c(\boldsymbol{r})$, respectively. Here, $\boldsymbol{\sigma}$ is the Pauli matrix, and $d=\left\{d_{\uparrow},d_{\downarrow}\right\}^{\rm T}$ and $c(\boldsymbol{r})=\left\{c_{\uparrow}(\boldsymbol{r}),c_{\downarrow}(\boldsymbol{r})\right\}^{\rm T}$ are the annihilation operators at the impurity site and in the superconductors.

The spatial spin–spin correlation function is given by

$$J_{uv}(\boldsymbol{r})=\langle S^{u}_{\rm c}(\boldsymbol{r})S^{v}_{\rm d}(0)\rangle\,, \tag{23}$$

with $u,v=x,y,z$, and $\langle\cdots\rangle$ means the ground state average. When the Kondo effect occurs, the magnetic impurity spin is completely dissolved by quantum fluctuations below the Kondo temperature, and this process is accompanied by the formation of Kondo cloud, which can be characterized by the spin–spin correlation function. This Kondo screening cloud in an s-wave superconductor has been studied before,[23] and the integration of this spin–spin correlation in the D-dimensional coordinate space can be used to measure the strength of the Kondo screening. The spatial patterns of the spin–spin correlations are mainly determined by the symmetry of the host materials, so we start with the symmetry analysis of the superconducting states. H_0, which describes the superconductor with mixed s- and p-wave pairings, is given in Eqs. (1)–(4), and one can easily find that H_0 is rotational symmetric about the z-axis. Considering this rotational symmetry, we have $J_{uv}(\boldsymbol{r})=J_{u'v'}(\boldsymbol{r}')$ if $u'=\mathcal{R}^{z}(\eta)u$, $v'=\mathcal{R}^{z}(\eta)v$, $\boldsymbol{r}'=\mathcal{R}^{z}(\eta)\boldsymbol{r}$, where $\mathcal{R}^{z}(\eta)$ is a rotation operator of angle η along the z-axis. Hence the various components of the spin–spin correlation shall obey $J_{xx}(\boldsymbol{r})=J_{yy}(\mathcal{R}^{z}(\frac{\pi}{2})\boldsymbol{r})$, $J_{xz}(\boldsymbol{r})=J_{yz}(\mathcal{R}^{z}(\frac{\pi}{2})\boldsymbol{r})$, $J_{zx}(\boldsymbol{r})=J_{zy}(\mathcal{R}^{z}(\frac{\pi}{2})\boldsymbol{r})$. When $v_z=0$, the system preserves time-reversal symmetry (TRS, $\mathcal{T}$), whereas finite v_z breaks the TRS. However, the system is still invariant under combined operations $\mathcal{T}\mathcal{R}^{x}(\pi)$ and $\mathcal{T}\mathcal{R}^{y}(\pi)$. Due to these symmetries, the off-diagonal terms have following properties along the x- and y-axes: $J_{xy}(x,0)=J_{xy}(0,y)=J_{xz}(x,0)=J_{yz}(0,y)$. The RSOC breaks the SU(2) symmetry, so the off-diagonal terms are in general nonzero in the x–y plane and $J_{xy}(\boldsymbol{r})=J_{yx}(\boldsymbol{r})$, $J_{xz}(\boldsymbol{r})=-J_{zx}(\boldsymbol{r})$, $J_{yz}(\boldsymbol{r})=-J_{zy}(\boldsymbol{r})$ if $v_z=0$.

In the orbital angular momentum representation, we only consider the total angular momentum $j=m+\sigma=\pm1/2$, so only the orbits of quantum number $m=0,\pm1$ are relevant to the Anderson impurity scattering. The spin–spin correlations are given by

$$\begin{aligned}
J_{xx}(\boldsymbol{r}) &= \sum_{mn}[C_{11}(\boldsymbol{r},m,n)+C_{12}(\boldsymbol{r},m,n)\\
&\quad +C_{13}(\boldsymbol{r},m,n)+C_{14}(\boldsymbol{r},m,n)]\,{\rm e}^{-{\rm i}(m\varphi-n\varphi)},\\
J_{yy}(\boldsymbol{r}) &= -\sum_{mn}[C_{11}(\boldsymbol{r},m,n)-C_{12}(\boldsymbol{r},m,n)\\
&\quad -C_{13}(\boldsymbol{r},m,n)+C_{14}(\boldsymbol{r},m,n)]\,{\rm e}^{-{\rm i}(m\varphi-n\varphi)},\\
J_{zz}(\boldsymbol{r}) &= \sum_{mn}[C_{41}(\boldsymbol{r},m,n)-C_{42}(\boldsymbol{r},m,n)\\
&\quad -C_{43}(\boldsymbol{r},m,n)+C_{44}(\boldsymbol{r},m,n)]\,{\rm e}^{-{\rm i}(m\varphi-n\varphi)},\\
J_{xy}(\boldsymbol{r}) &= -{\rm i}\sum_{mn}[C_{11}(\boldsymbol{r},m,n)-C_{12}(\boldsymbol{r},m,n)\\
&\quad +C_{13}(\boldsymbol{r},m,n)-C_{14}(\boldsymbol{r},m,n)]\,{\rm e}^{-{\rm i}(m\varphi-n\varphi)},\\
J_{yx}(\boldsymbol{r}) &= -{\rm i}\sum_{mn}[C_{11}(\boldsymbol{r},m,n)+C_{12}(\boldsymbol{r},m,n)\\
&\quad -C_{13}(\boldsymbol{r},m,n)-C_{14}(\boldsymbol{r},m,n)]\,{\rm e}^{-{\rm i}(m\varphi-n\varphi)},\\
J_{xz}(\boldsymbol{r}) &= \sum_{mn}[C_{21}(\boldsymbol{r},m,n)-C_{22}(\boldsymbol{r},m,n)\\
&\quad +C_{23}(\boldsymbol{r},m,n)-C_{24}(\boldsymbol{r},m,n)]\,{\rm e}^{-{\rm i}(m\varphi-n\varphi)},\\
J_{zx}(\boldsymbol{r}) &= \sum_{mn}[C_{31}(\boldsymbol{r},m,n)+C_{32}(\boldsymbol{r},m,n)\\
&\quad -C_{33}(\boldsymbol{r},m,n)-C_{34}(\boldsymbol{r},m,n)]\,{\rm e}^{-{\rm i}(m\varphi-n\varphi)},\\
J_{yz}(\boldsymbol{r}) &= -{\rm i}\sum_{mn}[C_{21}(\boldsymbol{r},m,n)-C_{22}(\boldsymbol{r},m,n)\\
&\quad -C_{23}(\boldsymbol{r},m,n)+C_{24}(\boldsymbol{r},m,n)]\,{\rm e}^{-{\rm i}(m\varphi-n\varphi)},\\
J_{zy}(\boldsymbol{r}) &= -{\rm i}\sum_{mn}[C_{31}(\boldsymbol{r},m,n)-C_{32}(\boldsymbol{r},m,n)\\
&\quad -C_{33}(\boldsymbol{r},m,n)+C_{34}(\boldsymbol{r},m,n)]\,{\rm e}^{-{\rm i}(m\varphi-n\varphi)},
\end{aligned}\tag{24}$$

where m and n are the orbital angular momentum quantum number, φ is the polar angle of spatial coordinate $\boldsymbol{r}$, that is, $\varphi=\arctan(r_y/r_x)$. The parameters $C_{ii'}(\boldsymbol{r},m,n)$ $(i,i'=1,2,3,4)$ are defined in Appendix B. If $v_z=0$, it is easy to obtain $\beta_{1k}=\beta_{-1k}$, and then $C_{12}(\boldsymbol{r},m,n)=C_{13}(\boldsymbol{r},m,n)$ such that $J_{xy}(\boldsymbol{r})=J_{yx}(\boldsymbol{r})$. In all the results of spin–spin correlation function we present below, the binding energy is fixed as $\Delta_{\rm b}=5\Delta_0$. Actually the magnitude of the binding energy depends on various parameters of the Hamiltonian. However, the spatial patterns of the spin–spin correlation function are not much affected by the values of $\Delta_{\rm b}$ except the magnitudes.

In Fig. 2 we show the diagonal and off-diagonal terms of the spin–spin correlation between the magnetic impurity and the conduction electrons in the coordinate space. Here we fix $V=27.5\Delta_0$, $\lambda=50\Delta_0$, $\Delta=\Delta_0$, and $v_z=0$, and $k_{\rm c}$ is the momentum cutoff chosen with respect to the energy cutoff W. One can see that $J_{xx}(\boldsymbol{r})$ and $J_{yy}(\boldsymbol{r})$ are anisotropic, while $J_{zz}(\boldsymbol{r})$ is isotropic for the diagonal term. In addition, $J_{yy}(r)$ can be obtained by rotating $\pi/2$ by $J_{xx}(\boldsymbol{r})$. For off-diagonal terms, $J_{yx}(\boldsymbol{r})=J_{xy}(\boldsymbol{r})$, $J_{zx}(\boldsymbol{r})=-J_{xz}(\boldsymbol{r})$, and $J_{zy}(\boldsymbol{r})=-J_{yz}(\boldsymbol{r})$, and $J_{xz}(\boldsymbol{r})$ can be obtained with rotating $\pi/2$ angle by $J_{yz}(\boldsymbol{r})$. These results agree well with those of our symmetry analysis.

In Fig. 3 we show the decay of $J_{zz}(\boldsymbol{r})$ along the x-axis with different parameters of λ, Δ_0 and v_z for $V=27.5\Delta_0$. $J_{zz}(\boldsymbol{r})$ is rotational symmetric in the x–y plane. When $v_z=0$, $J_{yy}(\boldsymbol{r})=J_{zz}(\boldsymbol{r})$ along the x-axis and $J_{xx}(\boldsymbol{r})=J_{zz}(\boldsymbol{r})$ along the y-axis. One can see that $J_{zz}(\boldsymbol{r})$ decays faster with the increase of λ, energy gap Δ and magnetic field v_z. Numerical renor-

malization group study shows that in an s-wave superconductor, the Kondo screening cloud is formed in both the screened and unscreened phases, and decays with respect to $1/r$ in the vicinity of the magnetic impurity, and the decay rate in larger distances depends on the magnitude of the superconducting gap.[23]

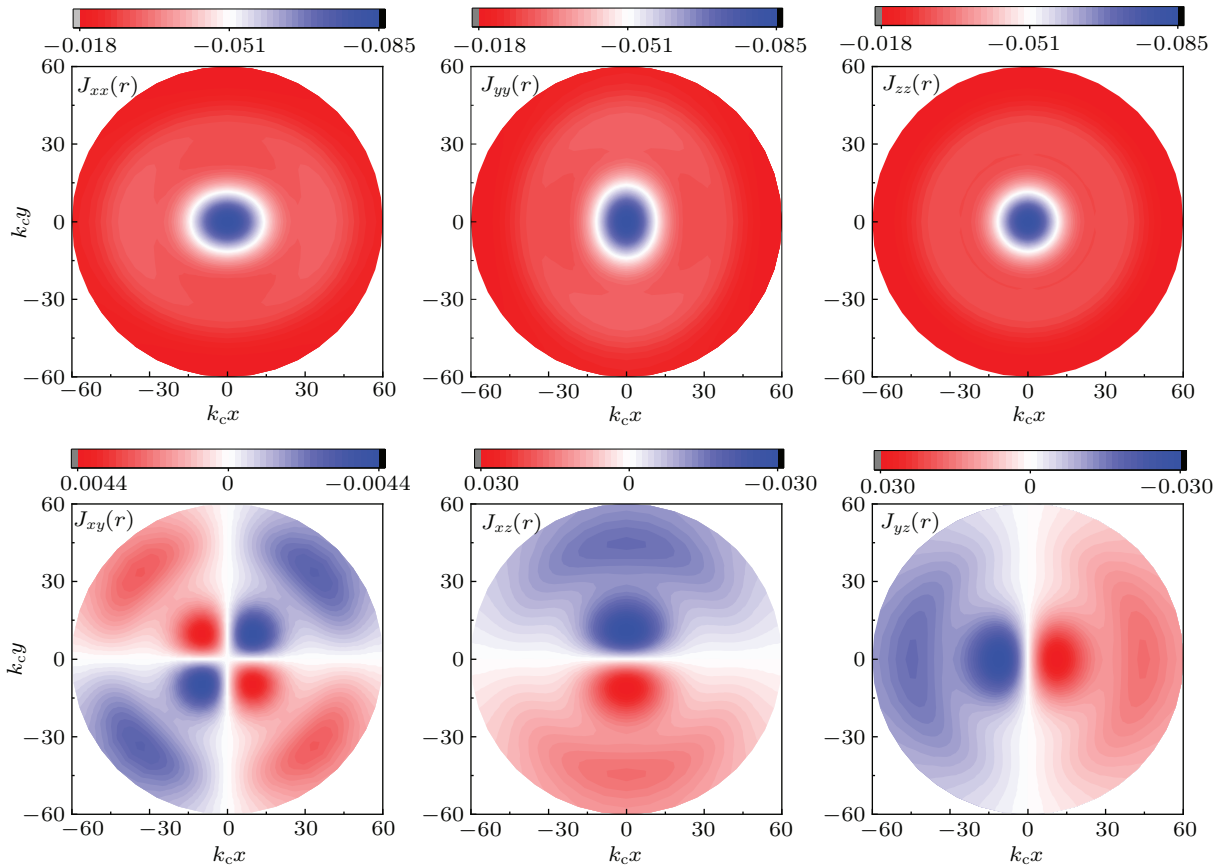


Fig. 2. Terms of the spin–spin correlation $J_{uv}(\boldsymbol{r})(u,v=x,y,z)$ in coordinate space for $V=27.5\Delta_0$, $\lambda=50\Delta_0$, $\Delta=\Delta_0$, and $v_z=0$, where k_c is the momentum cutoff chosen with respect to the energy cutoff W. The off-diagonal terms not shown here have the relations $J_{yx}(\boldsymbol{r})=J_{xy}(\boldsymbol{r})$, $J_{zx}(\boldsymbol{r})=-J_{xz}(\boldsymbol{r})$, and $J_{zy}(\boldsymbol{r})=-J_{yz}(\boldsymbol{r})$.

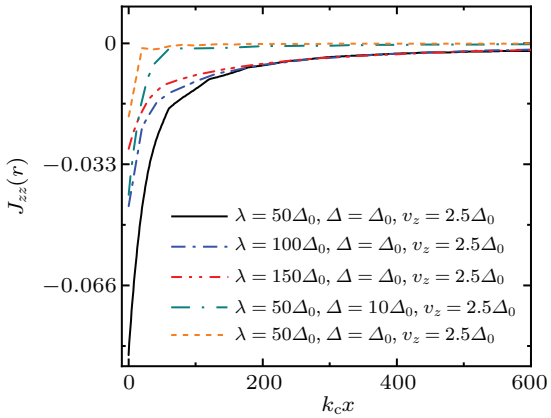


Fig. 3. Spatial decay behavior of $J_{zz}(\boldsymbol{r})$ along the x-axis with different parameters of λ, Δ_0 and v_z for $V=27.5\Delta_0$.

In Fig. 4 we show the off-diagonal terms corresponding to different parameters. In Fig. 4(a) (the left column) we use $\lambda=100\Delta_0$, $\Delta=\Delta_0$ and in Fig. 4(b) (the right column) $\lambda=50\Delta_0$, $\Delta=5\Delta_0$. The hybridization is $V=27.5\Delta_0$ and the Zeeman field is $v_z=0$. In comparison with Fig. 2, we can see that if λ or Δ increases, the off-diagonal terms become weaker, and the spatial patterns are qualitatively the same since λ and Δ do not break any symmetries. We still have $J_{yx}(\boldsymbol{r})=J_{xy}(\boldsymbol{r})$, $J_{zx}(\boldsymbol{r})=-J_{xz}(\boldsymbol{r})$, and $J_{zy}(\boldsymbol{r})=-J_{yz}(\boldsymbol{r})$, and $J_{yz}(\boldsymbol{r})$ can be obtained by rotating $J_{xz}(\boldsymbol{r})$ by angle $\pi/2$ about the z-axis.

In Fig. 5, we mainly investigate the effect of the Zeeman field on the spatial patterns of the spin–spin correlation function. We show $J_{xx}(\boldsymbol{r})$ and off-diagonal terms corresponding to different v_z, in which $\lambda=50\Delta_0$, $\Delta=\Delta_0$ and $V=27.5\Delta_0$. In Figs. 5(a) and 5(b) we choose $v_z=2.5\Delta_0$ and $v_z=50\Delta_0$, respectively. Compared with Fig. 2, when the Zeeman field v_z becomes finite, the spin–spin correlation components become weaker. Moreover, the finite Zeeman field removes the spin degeneracy of the quasiparticles excited in the triplet states, and induces extra asymmetries to the off-diagonal terms. Very distinctly from the $v_z=0$ case, we now have $J_{xz}(\boldsymbol{r})\neq-J_{zx}(\boldsymbol{r})$ and $J_{yz}(\boldsymbol{r})\neq-J_{zy}(\boldsymbol{r})$ for the two off-diagonal terms. This behavior is even more pronounced when the Zeeman field becomes stronger. However, the system remains invariant under the rotation about the z-axis and the combined operations $\mathcal{TR}^{\S}(\pi)$, $\mathcal{TR}^{y}(\pi)$. Thus, the symmetry for the spin–spin correlation of the diagonal terms is unchanged and we still have $J_{xx}(\boldsymbol{r})=J_{yy}(\mathcal{R}^{z}(\frac{\pi}{2})\boldsymbol{r})$. The same holds for off-diagonal terms that $J_{xz}(\boldsymbol{r})=J_{yz}(\mathcal{R}^{z}(\frac{\pi}{2})\boldsymbol{r})$, $J_{zx}(\boldsymbol{r})=J_{zy}(\mathcal{R}^{z}(\frac{\pi}{2})\boldsymbol{r})$.

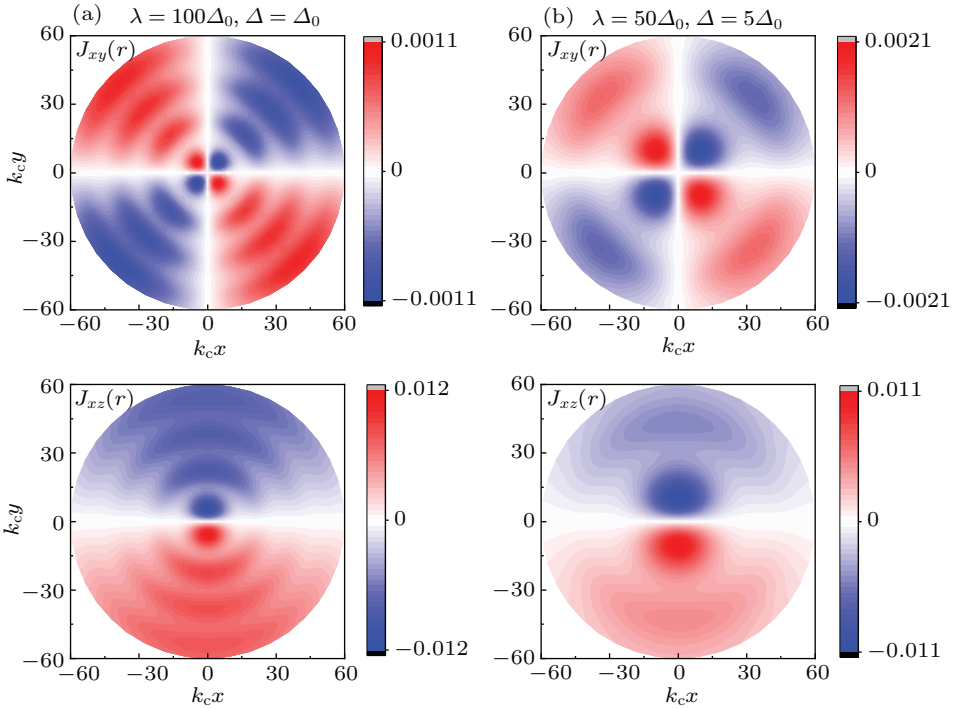


Fig. 4. Off-diagonal terms of spin–spin correlation for (a) $\lambda = 100\Delta_0$, $\Delta = \Delta_0$ (the left column) and (b) $\lambda = 50\Delta_0$, $\Delta = 5\Delta_0$ (the right column). The hybridization is $V = 27.5\Delta_0$, and Zeeman field is $v_z = 0$. $J_{yz}(\boldsymbol{r}) = J_{xz}(\mathcal{R}^z(\pi/2)\boldsymbol{r})$, so it is not shown here.

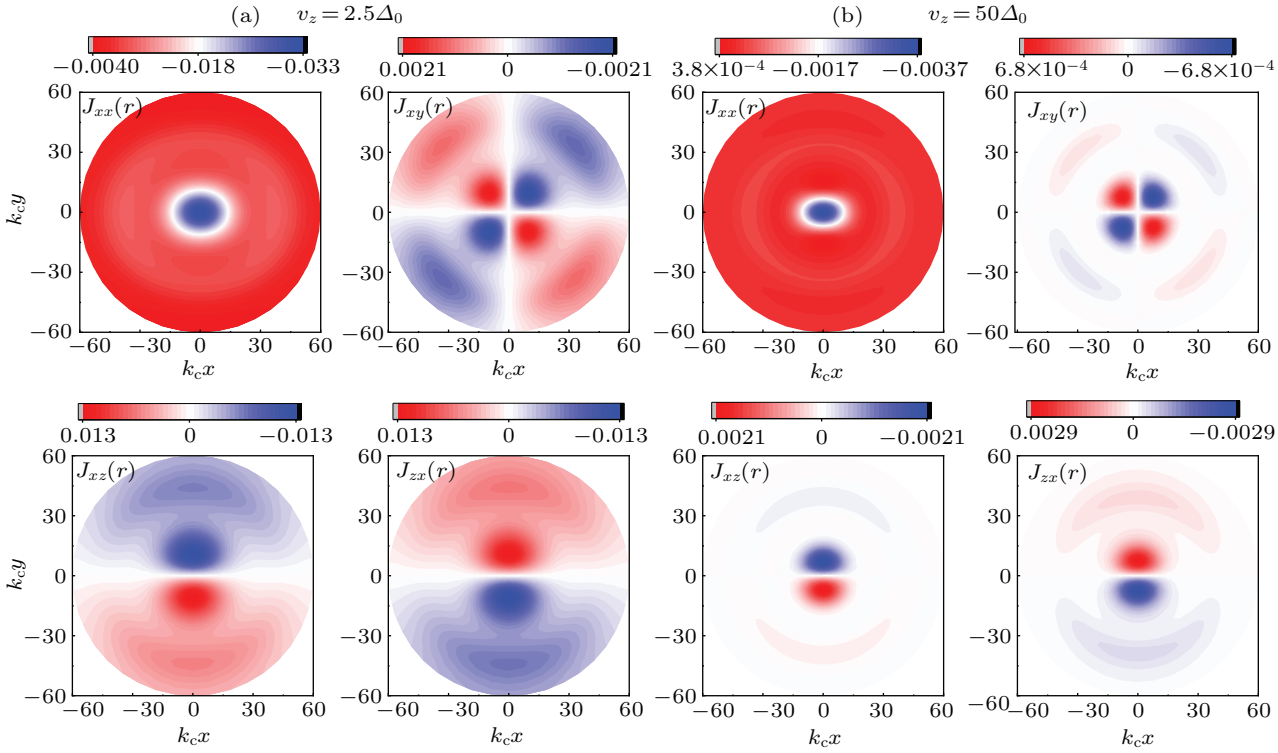


Fig. 5. The change of $J_{uv}(\boldsymbol{r})$ when $v_z \neq 0$, with $\lambda = 50\Delta_0$, $\Delta = \Delta_0$, $V = 27.5\Delta_0$. The Zeeman field is (a) $v_z = 2.5\Delta_0$ and (b) $v_z = 50\Delta_0$.

5. Discussion and conclusion

In summary, we have utilized the variational wavefunction method to study the binding energy and the spatial anisotropy of the Kondo screening cloud in a superconductor with coexisting s-wave and p-wave pairing states. The host system is constructed from a combination of an s-wave superconductor, a ferromagnet which produces a Zeeman field, and a semiconductor with RSOC. The ground state of a magnetic impurity in a conventional s-wave superconductor or a intrinsic p-wave is a well-studied problem. When the two pairings are mixed, the Kondo screenings show interesting features. We concentrate on the binding energy and the spin–spin correlation function which describes the so-called Kondo

screening cloud, and systematically study the effects of the RSOC, Zeeman field, and superconducting gap size on the Kondo screening. From the results of the binding energy calculations, we find that Kondo screening is favored for strong RSOC and weak Zeeman field cases. In general, the binding energy grows monotonically with the hybridization strength, and decreases when the superconducting gap increases, which is in consistence with the picture that the ground state is determined by the competition between $T_{\rm K}$ and Δ. Due to the RSOC, the diagonal components become anisotropic, and various off-diagonal components emerge. The spin–spin correlation decays fast in the real space, and Zeeman field induces extra asymmetry to the off-diagonal components. So far, we assume a singlet ground state, which is reasonable if $V \gg \Delta$. If we fix other parameters and gradually increase V, the ground is expected to experience a transition from a magnetic doublet to a Kondo singlet. In the binding energy calculations, this transition can be detected by comparing the binding energy in the two ground states, and will be investigated in our future work.

Appendix A

By diagonalizing the Hamiltonian in Eq. (11), one can obtain the band structure

$$E_{ki} = \pm\sqrt{\lambda^2 k^2 + v_z^2} \pm \sqrt{\Delta^2 + \varepsilon_k^2}. \tag{A1}$$

We label the excitation energies in an increasing order as $E_{k2}, E_{k3}, E_{k4}, E_{k1}$

For $E_{k1} = \sqrt{\lambda^2 k^2 + v_z^2} + \sqrt{\Delta^2 + \varepsilon_k^2}$, the corresponding eigen-vector components are

$$\begin{aligned}
\Phi_{11} &= -\frac{\varepsilon_k + \sqrt{\Delta^2 + \varepsilon_k^2}}{\sqrt{(\varepsilon_k + \sqrt{\Delta^2 + \varepsilon_k^2})^2 + \Delta^2}}, \\
\Phi_{31} &= \frac{\Delta}{\sqrt{(\varepsilon_k + \sqrt{\Delta^2 + \varepsilon_k^2})^2 + \Delta^2}}, \\
\Phi_{21} &= \Phi_{41} = 0.
\end{aligned} \tag{A2}$$

For $E_{k2} = -\sqrt{\lambda^2 k^2 + v_z^2} - \sqrt{\Delta^2 + \varepsilon_k^2}$, the eigen-vector components are

$$\begin{aligned}
\Phi_{22} &= -\frac{\varepsilon_k + \sqrt{\Delta^2 + \varepsilon_k^2}}{\sqrt{(\varepsilon_k + \sqrt{\Delta^2 + \varepsilon_k^2})^2 + \Delta}^2} = \Phi_{11}, \\
\Phi_{42} &= \frac{\Delta}{\sqrt{(\varepsilon_k + \sqrt{\Delta^2 + \varepsilon_k^2})^2 + \Delta^2}} = \Phi_{31}, \\
\Phi_{12} &= \Phi_{32} = 0.
\end{aligned} \tag{A3}$$

We always have $E_{k3} + E_{k4} = 0$, but the signs of E_{k3} and E_{k4} depend on the parameters and momentum k. If $-\sqrt{\lambda^2 k^2 + v_z^2} + \sqrt{\Delta^2 + \varepsilon_k^2} < 0$, then $E_{k3} = -\sqrt{\lambda^2 k^2 + v_z^2} + \sqrt{\Delta^2 + \varepsilon_k^2}$, $E_{k4} = \sqrt{\lambda^2 k^2 + v_z^2} - \sqrt{\Delta^2 + \varepsilon_k^2}$ and then the corresponding eigen-vector components are

$$\begin{aligned}
\Phi_{23} = \Phi_{14} &= -\frac{\varepsilon_k - \sqrt{\Delta^2 + \varepsilon_k^2}}{\sqrt{(\varepsilon_k - \sqrt{\Delta^2 + \varepsilon_k^2})^2 + \Delta^2}}, \\
\Phi_{43} = \Phi_{34} &= \frac{\Delta}{\sqrt{(\varepsilon_k - \sqrt{\Delta^2 + \varepsilon_k^2})^2 + \Delta^2}}, \\
\Phi_{13} = \Phi_{33} &= \Phi_{24} = \Phi_{44} = 0.
\end{aligned} \tag{A4}$$

Otherwise, $E_{k3} = \sqrt{\lambda^2 k^2 + v_z^2} - \sqrt{\Delta^2 + \varepsilon_k^2}$, $E_{k4} = -\sqrt{\lambda^2 k^2 + v_z^2} + \sqrt{\Delta^2 + \varepsilon_k^2}$,

$$\begin{aligned}
\Phi_{13} = \Phi_{24} &= -\frac{\varepsilon_k - \sqrt{\Delta^2 + \varepsilon_k^2}}{\sqrt{(\varepsilon_k - \sqrt{\Delta^2 + \varepsilon_k^2})^2 + \Delta^2}}, \\
\Phi_{33} = \Phi_{44} &= \frac{\Delta}{\sqrt{(\varepsilon_k - \sqrt{\Delta^2 + \varepsilon_k^2})^2 + \Delta^2}}, \\
\Phi_{23} = \Phi_{43} &= \Phi_{14} = \Phi_{34} = 0.
\end{aligned} \tag{A5}$$

Finally, the unitary transformation used in Eq. (13) is given by

$$\mathcal{U} = \begin{pmatrix} \Phi_{11} & 0 & \Phi_{13} & \Phi_{14} \\ 0 & \Phi_{22} & \Phi_{23} & \Phi_{24} \\ \Phi_{31} & 0 & \Phi_{33} & \Phi_{34} \\ 0 & \Phi_{42} & \Phi_{43} & \Phi_{44} \end{pmatrix}. \tag{A6}$$

Appendix B

One of the diagonal components of the spin–spin correlation, $J_{xx}(\boldsymbol{r})$ is given by

$$\begin{aligned}
J_{xx}(\boldsymbol{r}) &= \langle S_{\rm c}^x(\boldsymbol{r}) S_{\rm d}^x(0)\rangle = \frac{1}{4}\left\langle (c_\uparrow^\dagger(\boldsymbol{r}) c_\downarrow(\boldsymbol{r}) + c_\downarrow^\dagger(\boldsymbol{r}) c_\uparrow(\boldsymbol{r}))(d_\uparrow^\dagger d_\downarrow + d_\downarrow^\dagger d_\uparrow)\right\rangle \\
&= \frac{1}{4}\left\langle c_\uparrow^\dagger(\boldsymbol{r}) c_\downarrow(\boldsymbol{r}) d_\uparrow^\dagger d_\downarrow + c_\uparrow^\dagger(\boldsymbol{r}) c_\downarrow(\boldsymbol{r}) d_\downarrow^\dagger d_\uparrow + c_\downarrow^\dagger(\boldsymbol{r}) c_\uparrow(\boldsymbol{r}) d_\uparrow^\dagger d_\downarrow + c_\downarrow^\dagger(\boldsymbol{r}) c_\uparrow(\boldsymbol{r}) d_\downarrow^\dagger d_\uparrow\right\rangle \\
&= \frac{1}{32\pi^3 N}\int \sqrt{kk'}\,{\rm d}k\,{\rm d}k' \int_0^{2\pi} {\rm d}\theta_{k1}\,{\rm d}\theta_{k'2}\, {\rm e}^{-{\rm i}[kr\cos\theta_{k1} - k'r\cos\theta_{k'2}]} \sum_{mn} {\rm e}^{-{\rm i}(m\theta_{k1} - n\theta_{k'2})}\, {\rm e}^{-{\rm i}(m\varphi - n\varphi)}
\end{aligned}$$

$$\times\left\langle c_{k\uparrow}^{m\dagger}c_{k'\downarrow}^{n}d_{\uparrow}^{\dagger}d_{\downarrow}+c_{k\uparrow}^{m\dagger}c_{k'\downarrow}^{n}d_{\downarrow}^{\dagger}d_{\uparrow}+c_{k\downarrow}^{m\dagger}c_{k'\uparrow}^{n}d_{\uparrow}^{\dagger}d_{\downarrow}+c_{k\downarrow}^{m\dagger}c_{k'\uparrow}^{n}d_{\downarrow}^{\dagger}d_{\uparrow}\right\rangle$$
$$=\sum_{mn}[C_{11}(\boldsymbol{r},m,n)+C_{12}(\boldsymbol{r},m,n)+C_{13}(\boldsymbol{r},m,n)+C_{14}(\boldsymbol{r},m,n)]\,\mathrm{e}^{-\mathrm{i}(m\varphi-n\varphi)}, \tag{B1}$$

with

$$C_{11}(\boldsymbol{r},m,n)=\frac{1}{32\pi^3N}\int\sqrt{kk'}\,\mathrm{d}k\,\mathrm{d}k'\int_0^{2\pi}\mathrm{d}\theta_{k1}\,\mathrm{d}\theta_{k'2}\,\mathrm{e}^{-\mathrm{i}[kr\cos\theta_{k1}-k'r\cos\theta_{k'2}]}\,\mathrm{e}^{-\mathrm{i}(m\theta_{k1}-n\theta_{k'2})}\left\langle c_{k\uparrow}^{m\dagger}c_{k'\downarrow}^{n}d_{\uparrow}^{\dagger}d_{\downarrow}\right\rangle$$
$$=A_{kr}\,\mathrm{e}^{-\mathrm{i}(m\theta_{k1}-n\theta_{k'2})}\left\langle c_{k\uparrow}^{m\dagger}c_{k'\downarrow}^{n}d_{\uparrow}^{\dagger}d_{\downarrow}\right\rangle, \tag{B2}$$

$$C_{12}(\boldsymbol{r},m,n)=\frac{1}{32\pi^3N}\int\sqrt{kk'}\,\mathrm{d}k\,\mathrm{d}k'\int_0^{2\pi}\mathrm{d}\theta_{k1}\,\mathrm{d}\theta_{k'2}\,\mathrm{e}^{-\mathrm{i}[kr\cos\theta_{k1}-k'r\cos\theta_{k'2}]}\,\mathrm{e}^{-\mathrm{i}(m\theta_{k1}-n\theta_{k'2})}\left\langle c_{k\uparrow}^{m\dagger}c_{k'\downarrow}^{n}d_{\downarrow}^{\dagger}d_{\uparrow}\right\rangle$$
$$=A_{kr}\,\mathrm{e}^{-\mathrm{i}(m\theta_{k1}-n\theta_{k'2})}\left\langle c_{k\uparrow}^{m\dagger}c_{k'\downarrow}^{n}d_{\downarrow}^{\dagger}d_{\uparrow}\right\rangle, \tag{B3}$$

$$C_{13}(\boldsymbol{r},m,n)=\frac{1}{32\pi^3N}\int\sqrt{kk'}\,\mathrm{d}k\,\mathrm{d}k'\int_0^{2\pi}\mathrm{d}\theta_{k1}\,\mathrm{d}\theta_{k'2}\,\mathrm{e}^{-\mathrm{i}[kr\cos\theta_{k1}-k'r\cos\theta_{k'2}]}\,\mathrm{e}^{-\mathrm{i}(m\theta_{k1}-n\theta_{k'2})}\left\langle c_{k\downarrow}^{m\dagger}c_{k'\uparrow}^{n}d_{\uparrow}^{\dagger}d_{\downarrow}\right\rangle$$
$$=A_{kr}\,\mathrm{e}^{-\mathrm{i}(m\theta_{k1}-n\theta_{k'2})}\left\langle c_{k\downarrow}^{m\dagger}c_{k'\uparrow}^{n}d_{\uparrow}^{\dagger}d_{\downarrow}\right\rangle, \tag{B4}$$

$$C_{14}(\boldsymbol{r},m,n)=\frac{1}{32\pi^3N}\int\sqrt{kk'}\,\mathrm{d}k\,\mathrm{d}k'\int_0^{2\pi}\mathrm{d}\theta_{k1}\,\mathrm{d}\theta_{k'2}\,\mathrm{e}^{-\mathrm{i}[kr\cos\theta_{k1}-k'r\cos\theta_{k'2}]}\,\mathrm{e}^{-\mathrm{i}(m\theta_{k1}-n\theta_{k'2})}\left\langle c_{k\downarrow}^{m\dagger}c_{k'\uparrow}^{n}d_{\downarrow}^{\dagger}d_{\uparrow}\right\rangle$$
$$=A_{kr}\,\mathrm{e}^{-\mathrm{i}(m\theta_{k1}-n\theta_{k'2})}\,\mathrm{e}^{-\mathrm{i}(m\theta_{k1}-n\theta_{k'2})}\left\langle c_{k\downarrow}^{m\dagger}c_{k'\uparrow}^{n}d_{\downarrow}^{\dagger}d_{\uparrow}\right\rangle, \tag{B5}$$

and

$$A_{kr}=\frac{1}{32\pi^3N}\int\sqrt{kk'}\,\mathrm{d}k\,\mathrm{d}k'\int_0^{2\pi}\mathrm{d}\theta_{k1}\,\mathrm{d}\theta_{k'2}\,\mathrm{e}^{-\mathrm{i}[kr\cos\theta_{k1}-k'r\cos\theta_{k'2}]}. \tag{B6}$$
$$\sum_{mn}C_{11}(\boldsymbol{r},m,n)\,\mathrm{e}^{-\mathrm{i}(m\varphi-n\varphi)}$$
$$=\sum_{mn}A_{kr}\,\mathrm{e}^{-\mathrm{i}(m\theta_{k1}-n\theta_{k'2})}\,\mathrm{e}^{-\mathrm{i}(m\varphi-n\varphi)}\langle c_{k\uparrow}^{m\dagger}c_{k'\downarrow}^{n}d_{\uparrow}^{\dagger}d_{\downarrow}\rangle$$
$$=\sum_{mn}\frac{A_{kr}}{2}\,\mathrm{e}^{-\mathrm{i}(m\theta_{k1}-n\theta_{k'2})}\,\mathrm{e}^{-\mathrm{i}(m\varphi-n\varphi)}\big\langle(\beta_{1k}\beta_{-1k'}c^{\dagger}_{1km+\frac{1}{2}}c_{1k'n-1+\frac{1}{2}}-\beta_{1k}\beta_{1k'}c^{\dagger}_{1km+\frac{1}{2}}c_{-1k'n-1+\frac{1}{2}}$$
$$+\beta_{-1k}\beta_{-1k'}c^{\dagger}_{-1km+\frac{1}{2}}c_{1k'n-1+\frac{1}{2}}-\beta_{-1k}\beta_{1k'}c^{\dagger}_{-1km+\frac{1}{2}}c_{-1k'n-1+\frac{1}{2}})d_{\uparrow}^{\dagger}d_{\downarrow}\big\rangle. \tag{B7}$$

To ensure that $j=1/2$, we only consider the coupling between $m=0,-1$ and $n=0,1$ for $C_{11}(\boldsymbol{r},m,n)$. Similarly, the rest components of the spin–spin correlation can be calculated, with

$$C_{21}(\boldsymbol{r},m,n)=\frac{1}{64\pi^3N}\int\sqrt{kk'}\,\mathrm{d}k\,\mathrm{d}k'\int_0^{2\pi}\mathrm{d}\theta_{k1}\,\mathrm{d}\theta_{k'2}\,\mathrm{e}^{-\mathrm{i}[kr\cos\theta_{k1}-k'r\cos\theta_{k'2}]}\,\mathrm{e}^{-\mathrm{i}(m\theta_{k1}-n\theta_{k'2})}\left\langle c_{k\uparrow}^{m\dagger}c_{k'\downarrow}^{n}d_{\uparrow}^{\dagger}d_{\uparrow}\right\rangle$$
$$=A_{kr}\,\mathrm{e}^{-\mathrm{i}(m\theta_{k1}-n\theta_{k'2})}\left\langle c_{k\uparrow}^{m\dagger}c_{k'\downarrow}^{n}d_{\uparrow}^{\dagger}d_{\uparrow}\right\rangle, \tag{B8}$$

$$C_{22}(\boldsymbol{r},m,n)=\frac{1}{64\pi^3N}\int\sqrt{kk'}\,\mathrm{d}k\,\mathrm{d}k'\int_0^{2\pi}\mathrm{d}\theta_{k1}\,\mathrm{d}\theta_{k'2}\,\mathrm{e}^{-\mathrm{i}[kr\cos\theta_{k1}-k'r\cos\theta_{k'2}]}\,\mathrm{e}^{-\mathrm{i}(m\theta_{k1}-n\theta_{k'2})}\left\langle c_{k\uparrow}^{m\dagger}c_{k'\downarrow}^{n}d_{\downarrow}^{\dagger}d_{\downarrow}\right\rangle$$
$$=A_{kr}\,\mathrm{e}^{-\mathrm{i}(m\theta_{k1}-n\theta_{k'2})}\left\langle c_{k\uparrow}^{m\dagger}c_{k'\downarrow}^{n}d_{\downarrow}^{\dagger}d_{\downarrow}\right\rangle, \tag{B9}$$

$$C_{23}(\boldsymbol{r},m,n)=\frac{1}{64\pi^3N}\int\sqrt{kk'}\,\mathrm{d}k\,\mathrm{d}k'\int_0^{2\pi}\mathrm{d}\theta_{k1}\,\mathrm{d}\theta_{k'2}\,\mathrm{e}^{-\mathrm{i}[kr\cos\theta_{k1}-k'r\cos\theta_{k'2}]}\,\mathrm{e}^{-\mathrm{i}(m\theta_{k1}-n\theta_{k'2})}\left\langle c_{k\downarrow}^{m\dagger}c_{k'\uparrow}^{n}d_{\uparrow}^{\dagger}d_{\uparrow}\right\rangle$$
$$=A_{kr}\,\mathrm{e}^{-\mathrm{i}(m\theta_{k1}-n\theta_{k'2})}\left\langle c_{k\downarrow}^{m\dagger}c_{k'\uparrow}^{n}d_{\uparrow}^{\dagger}d_{\uparrow}\right\rangle, \tag{B10}$$

$$C_{24}(\boldsymbol{r},m,n)=\frac{1}{64\pi^3N}\int\sqrt{kk'}\,\mathrm{d}k\,\mathrm{d}k'\int_0^{2\pi}\mathrm{d}\theta_{k1}\,\mathrm{d}\theta_{k'2}\,\mathrm{e}^{-\mathrm{i}[kr\cos\theta_{k1}-k'r\cos\theta_{k'2}]}\,\mathrm{e}^{-\mathrm{i}(m\theta_{k1}-n\theta_{k'2})}\left\langle c_{k\downarrow}^{m\dagger}c_{k'\uparrow}^{n}d_{\downarrow}^{\dagger}d_{\downarrow}\right\rangle$$
$$=A_{kr}\,\mathrm{e}^{-\mathrm{i}(m\theta_{k1}-n\theta_{k'2})}\,\mathrm{e}^{-\mathrm{i}(m\theta_{k1}-n\theta_{k'2})}\left\langle c_{k\downarrow}^{m\dagger}c_{k'\uparrow}^{n}d_{\downarrow}^{\dagger}d_{\downarrow}\right\rangle, \tag{B11}$$

$$C_{31}(\boldsymbol{r},m,n)=\frac{1}{64\pi^3N}\int\sqrt{kk'}\,\mathrm{d}k\,\mathrm{d}k'\int_0^{2\pi}\mathrm{d}\theta_{k1}\,\mathrm{d}\theta_{k'2}\,\mathrm{e}^{-\mathrm{i}[kr\cos\theta_{k1}-k'r\cos\theta_{k'2}]}\,\mathrm{e}^{-\mathrm{i}(m\theta_{k1}-n\theta_{k'2})}\left\langle c_{k\uparrow}^{m\dagger}c_{k'\uparrow}^{n}d_{\uparrow}^{\dagger}d_{\downarrow}\right\rangle$$
$$=A_{kr}\,\mathrm{e}^{-\mathrm{i}(m\theta_{k1}-n\theta_{k'2})}\left\langle c_{k\uparrow}^{m\dagger}c_{k'\uparrow}^{n}d_{\uparrow}^{\dagger}d_{\downarrow}\right\rangle, \tag{B12}$$

$$C_{32}(\boldsymbol{r},m,n)=\frac{1}{64\pi^3N}\int\sqrt{kk'}\,\mathrm{d}k\,\mathrm{d}k'\int_0^{2\pi}\mathrm{d}\theta_{k1}\,\mathrm{d}\theta_{k'2}\,\mathrm{e}^{-\mathrm{i}[kr\cos\theta_{k1}-k'r\cos\theta_{k'2}]}\,\mathrm{e}^{-\mathrm{i}(m\theta_{k1}-n\theta_{k'2})}\left\langle c_{k\uparrow}^{m\dagger}c_{k'\uparrow}^{n}d_{\downarrow}^{\dagger}d_{\uparrow}\right\rangle$$

$$= A_{kr}\,\mathrm{e}^{-\mathrm{i}(m\theta_{k1}-n\theta_{k'2})}\left\langle c^{m\dagger}_{k\uparrow}c^{n}_{k'\uparrow}d^{\dagger}_{\downarrow}d_{\uparrow}\right\rangle, \tag{B13}$$

$$C_{33}(\boldsymbol{r},m,n) = \frac{1}{64\pi^3 N}\int\sqrt{kk'}\,\mathrm{d}k\,\mathrm{d}k'\int_0^{2\pi}\mathrm{d}\theta_{k1}\,\mathrm{d}\theta_{k'2}\,\mathrm{e}^{-\mathrm{i}[kr\cos\theta_{k1}-k'r\cos\theta_{k'2}]}\,\mathrm{e}^{-\mathrm{i}(m\theta_{k1}-n\theta_{k'2})}\left\langle c^{m\dagger}_{k\downarrow}c^{n}_{k'\downarrow}d^{\dagger}_{\uparrow}d_{\downarrow}\right\rangle$$
$$= A_{kr}\,\mathrm{e}^{-\mathrm{i}(m\theta_{k1}-n\theta_{k'2})}\left\langle c^{m\dagger}_{k\downarrow}c^{n}_{k'\downarrow}d^{\dagger}_{\uparrow}d_{\downarrow}\right\rangle, \tag{B14}$$

$$C_{34}(\boldsymbol{r},m,n) = \frac{1}{64\pi^3 N}\int\sqrt{kk'}\,\mathrm{d}k\,\mathrm{d}k'\int_0^{2\pi}\mathrm{d}\theta_{k1}\,\mathrm{d}\theta_{k'2}\,\mathrm{e}^{-\mathrm{i}[kr\cos\theta_{k1}-k'r\cos\theta_{k'2}]}\,\mathrm{e}^{-\mathrm{i}(m\theta_{k1}-n\theta_{k'2})}\left\langle c^{m\dagger}_{k\downarrow}c^{n}_{k'\downarrow}d^{\dagger}_{\downarrow}d_{\uparrow}\right\rangle$$
$$= A_{kr}\,\mathrm{e}^{-\mathrm{i}(m\theta_{k1}-n\theta_{k'2})}\,\mathrm{e}^{-\mathrm{i}(m\theta_{k1}-n\theta_{k'2})}\left\langle c^{m\dagger}_{k\downarrow}c^{n}_{k'\downarrow}d^{\dagger}_{\downarrow}d_{\uparrow}\right\rangle, \tag{B15}$$

$$C_{41}(\boldsymbol{r},m,n) = \frac{1}{64\pi^3 N}\int\sqrt{kk'}\,\mathrm{d}k\,\mathrm{d}k'\int_0^{2\pi}\mathrm{d}\theta_{k1}\,\mathrm{d}\theta_{k'2}\,\mathrm{e}^{-\mathrm{i}[kr\cos\theta_{k1}-k'r\cos\theta_{k'2}]}\,\mathrm{e}^{-\mathrm{i}(m\theta_{k1}-n\theta_{k'2})}\left\langle c^{m\dagger}_{k\uparrow}c^{n}_{k'\uparrow}d^{\dagger}_{\uparrow}d_{\uparrow}\right\rangle$$
$$= A_{kr}\,\mathrm{e}^{-\mathrm{i}(m\theta_{k1}-n\theta_{k'2})}\left\langle c^{m\dagger}_{k\uparrow}c^{n}_{k'\uparrow}d^{\dagger}_{\uparrow}d_{\uparrow}\right\rangle, \tag{B16}$$

$$C_{42}(\boldsymbol{r},m,n) = \frac{1}{64\pi^3 N}\int\sqrt{kk'}\,\mathrm{d}k\,\mathrm{d}k'\int_0^{2\pi}\mathrm{d}\theta_{k1}\,\mathrm{d}\theta_{k'2}\,\mathrm{e}^{-\mathrm{i}[kr\cos\theta_{k1}-k'r\cos\theta_{k'2}]}\,\mathrm{e}^{-\mathrm{i}(m\theta_{k1}-n\theta_{k'2})}\left\langle c^{m\dagger}_{k\uparrow}c^{n}_{k'\uparrow}d^{\dagger}_{\downarrow}d_{\downarrow}\right\rangle$$
$$= A_{kr}\,\mathrm{e}^{-\mathrm{i}(m\theta_{k1}-n\theta_{k'2})}\left\langle c^{m\dagger}_{k\uparrow}c^{n}_{k'\uparrow}d^{\dagger}_{\downarrow}d_{\downarrow}\right\rangle, \tag{B17}$$

$$C_{43}(\boldsymbol{r},m,n) = \frac{1}{64\pi^3 N}\int\sqrt{kk'}\,\mathrm{d}k\,\mathrm{d}k'\int_0^{2\pi}\mathrm{d}\theta_{k1}\,\mathrm{d}\theta_{k'2}\,\mathrm{e}^{-\mathrm{i}[kr\cos\theta_{k1}-k'r\cos\theta_{k'2}]}\,\mathrm{e}^{-\mathrm{i}(m\theta_{k1}-n\theta_{k'2})}\left\langle c^{m\dagger}_{k\downarrow}c^{n}_{k'\downarrow}d^{\dagger}_{\uparrow}d_{\uparrow}\right\rangle$$
$$= A_{kr}\,\mathrm{e}^{-\mathrm{i}(m\theta_{k1}-n\theta_{k'2})}\left\langle c^{m\dagger}_{k\downarrow}c^{n}_{k'\downarrow}d^{\dagger}_{\uparrow}d_{\uparrow}\right\rangle, \tag{B18}$$

$$C_{44}(\boldsymbol{r},m,n) = \frac{1}{64\pi^3 N}\int\sqrt{kk'}\,\mathrm{d}k\,\mathrm{d}k'\int_0^{2\pi}\mathrm{d}\theta_{k1}\,\mathrm{d}\theta_{k'2}\,\mathrm{e}^{-\mathrm{i}[kr\cos\theta_{k1}-k'r\cos\theta_{k'2}]}\,\mathrm{e}^{-\mathrm{i}(m\theta_{k1}-n\theta_{k'2})}\left\langle c^{m\dagger}_{k\downarrow}c^{n}_{k'\downarrow}d^{\dagger}_{\downarrow}d_{\downarrow}\right\rangle$$
$$= A_{kr}\,\mathrm{e}^{-\mathrm{i}(m\theta_{k1}-n\theta_{k'2})}\,\mathrm{e}^{-\mathrm{i}(m\theta_{k1}-n\theta_{k'2})}\left\langle c^{m\dagger}_{k\downarrow}c^{n}_{k'\downarrow}d^{\dagger}_{\downarrow}d_{\downarrow}\right\rangle. \tag{B19}$$

Acknowledgements

The computation is performed in the Supercomputer Center of Ningbo University.

Project supported by the Zhejiang Provincial Natural Science Foundation of China (Grant No. LY19A040003).

References

[1] Kondo J 1964 *Prog. Theor. Phys.* **32** 37
[2] Anderson P W 1961 *Phys. Rev.* **124** 41
[3] Wilson K G 1975 *Rev. Mod. Phys.* **47** 773
[4] Yu L 1965 *Acta Phys. Sin.* **21** 75 (in Chinese)
[5] Shiba H 1968 *Prog. Theor. Phys.* **40** 435
[6] Rusinov A I 1969 *Sov. Phys. JETP* **29** 1101
[7] Hudson E W, Lang K M, Madhavan V, Pan S H, Eisaki H, Uchida S and Davis J C 2001 *Nature* **411** 920
[8] Yazdani A, Howald C M, Lutz C P, KapitulniA k and Eigler D M 1999 *Phys. Rev. Lett.* **83** 176
[9] Hudson E W, Pan S H, Gupta A K, Ng K W and Davis J C 1999 *Science* **285** 88
[10] Pan S H, Hudson E W, Lang K M, Eisaki H, Uchida S and Davis J C 2000 *Nature* **403** 746
[11] Tsai W F, Zhang Y Y, Fang C and Hu J P 2009 *Phys. Rev. B* **80** 064513
[12] Bang Y K, Choi H Y and Won H 2009 *Phys. Rev. B* **79** 054529
[13] Akbari A, Eremin I and Thalmeier P 2010 *Phys. Rev. B* **81** 014524
[14] Zha G Q and Jin Y Y 2017 *Europhys. Lett.* **120** 27002
[15] Guo Y Wu, Li W and Chen Y 2017 *Front. Phys.* **12** 1
[16] Sau J D and Demler E 2013 *Phys. Rev. B* **88** 205402
[17] Fu Z G, Zhang P, Wang Z G and Li S S 2012 *J. Phys.: Condens. Matter* **24** 145502
[18] Chen L, Zhang Y L and Han R S 2019 *J. Phys.: Condens. Matter* **31** 505603
[19] Chen R, Zhou B and Xu D H 2018 *Phys. Rev. B* **97** 155152
[20] Ishii H 1978 *J. Low Temp. Phys.* **32** 457
[21] Barzykin V and Affleck I 1998 *Phys. Rev. B* **57** 432
[22] Borda L 2007 *Phys. Rev. B* **75** 041307
[23] Moca C P, Weymann I, Werner M A and Zaránd G 2021 *Phys. Rev. Lett.* **127** 186804
[24] Borzenets I V, Shim J, Chen J C H, Ludwig A, Wieck A D, Tarucha S, Sim H S and Yamamoto M 2020 *Nature* **579** 210
[25] Wang Rui, Su W, Zhu J X, Ting C S, Li H, Chen C F, Wang B and Wang X Q 2019 *Phys. Rev. Lett.* **122** 087001
[26] Li L, Sun J H, Su W, Wang Z H, Xu D H, Luo H G and Chen W Q 2021 *Phys. Rev. B* **103** 125144
[27] Varma C M and Yafet Y 1976 *Phys. Rev. B* **13** 2950
[28] Gunnarsson O and Schönhammer K 1983 *Phys. Rev. Lett.* **50** 604
[29] Aji V, Varma C M and Vekhter I 2008 *Phys. Rev. B* **77** 224426
[30] Feng X Y, Chen W Q, Gao J H, Wang Q H and Zhang F C 2010 *Phys. Rev. B* **81** 235411
[31] Sun J H, Xu D H, Zhang F C and Zhou Y 2015 *Phys. Rev. B* **92** 195124
[32] Sun J H, Wang L J, Hu X T, Li L and Xu D H 2018 *Phys. Rev. B* **97** 035130
[33] Wang L J, Hu X T, Li L, Xu D H, Sun J H and Chen W Q 2019 *Phys. Rev. B* **99** 235108
[34] Yang X R, Huang Z Z, Wang W S and Sun J H 2021 *Chin. Phys. B* **30** 067103
[35] Deng Y H, Lü H F, K S S, Guo Y and Zhang H W 2018 *J. Phys.: Condens. Matter* **30** 435602
[36] Hone D 1967 *Solid State Commun.* **5** 705
[37] Simonin J and Allub R 1995 *Phys. Rev. Lett.* **74** 466
[38] Simon M E and Varma C M 1999 *Phys. Rev. B* **60** 9744
[39] Rozhkov A V and Arovas D P 2000 *Phys. Rev. B* **62** 6687
[40] Gor'kov L P and Rashba E I 2001 *Phys. Rev. Lett.* **87** 037004
[41] Frigeri P A, Agterberg D F, Koga A and Sigrist M 2004 *Phys. Rev. Lett.* **92** 097001
[42] Frigeri P A, Agterberg D F, Koga A and Sigrist M 2004 *Phys. Rev. Lett.* **93** 099903
[43] Sau J D, Lutchyn R M, Tewari S and Sarma S D 2010 *Phys. Rev. Lett.* **104** 040502
[44] Lutchyn R M, Sau J D and Sarma S D 2010 *Phys. Rev. Lett.* **105** 077001
[45] Ojanen T and Kitagawa T 2012 *Phys. Rev. B* **85** 161202
[46] Wong A, Ulloa S E, Sandler N and Ingersent K 2016 *Phys. Rev. B* **93** 075148
[47] Allison G, Fujita T, Morimoto K, Teraoka S, Larsson M, Kiyama H, Oiwa A, Haffouz S, Austing D G, Ludwig D G, Wieck A D and Tarucha S 2014 *Phys. Rev. B* **90** 235310
[48] Žitko R and Bonča J 2011 *Phys. Rev. B* **84** 193411
[49] Zarea M, Ulloa S E and Sandler N 2012 *Phys. Rev. Lett.* **108** 046601
[50] Isaev L, Agterberg D F and Vekhter I 2012 *Phys. Rev. B* **85** 081107
[51] Fujimoto S 2008 *Phys. Rev. B* **77** 220501
[52] Zhang C W, Tewari S, Lutchyn R M and Sarma S D 2008 *Phys. Rev. Lett.* **101** 160401
[53] Alicea J 2010 *Phys. Rev. B* **81** 125318
[54] Alicea J 2012 *Rep. Prog. Phys.* **75** 076501
[55] Malecki J 2007 *J. Statist. Phys.* **129** 741